PAWAN KUMAR[1], ANSHUL YADAV[2], ARVIND KUMAR[1]*

ELECTRON BEAM PROCESSING OF SENSORS RELEVANT VACOFLUX-49 ALLOY: EXPERIMENTAL STUDIES OF THERMAL ZONES AND MICROSTRUCTURE

Vacoflux-49 (Fe-49% Co-49% V-2%) is used in torque, sonar and gyroscopic sensors applications due to excellent magnetic properties (high saturation magnetisation, low coercivity and high Curie temperature). In this study, the shape, size and characteristics of different thermal zones and the microstructural evolution during electron beam melting and welding of Vacoflux-49 material are studied. The experimental studies on melting have been carried out with under-focussed, focussed and over focussed electron beam. In the case of the under-focussed and over-focused beam, no evaporated zone is found. In the case of focussed beam, a shallow conical-shaped evaporated zone, a choked funnel-shaped fusion zone, a conical shaped partially melted zone and the heat-affected zone are observed. The solidified melt pool in terms of shape, size and microstructure of different zones are investigated for the focussed beam. The grains in the fusion zone appear wavy having crest and trough. The fusion zone microstructure also shows the formation of solidification rings. From the electron beam welding experiments performed for joining two Vacoflux-49 plates (continuous welding), it is found that the weldment shape is similar to the spot melting and re-solidification experiments. The grain growth in different zones in the welding sample is also examined.

Keywords: Electron beam processing, Sensors applications, Vacoflux-49, Solidification ring, Fusion zone, Wavy pattern

1. Introduction

A wide variety of alloys can be processed using electron beam (EB) economically due to the high scanning rates associated with EB processes. The process also offers a high degree of flexibility in using the heat source. The process can achieve high build rates owing to increased penetration depths and elevated scanning velocities involved in the process. When the EB beam hits a metal surface, the high energy density is able to melt and can even vaporise the material directly under the beam spot. Schultz [1] reported the formation of a weld pool in EB welding and studied the weld pool formation and energy transfer mechanism in EB welding extensively. Nakkalil et al. [2] studied the influence of solidification mode on the microstructure of HAZ in Ni-Fe base superalloy and found the extensive formation of liquid film on the HAZ grain boundaries primarily due to the complete constitutional liquation of pre-existing phosphides,

carbides and partial constitutional liquation of primary carbide. Petrov et al. [3] notably described the mechanism of energy transfer from an EB to a metal target and weld pool during EB welding using a collector for secondary emitted particles, light photodiodes and charge-coupled device (CCD) techniques. It was shown that the nature of the heat source in a weld pool is non-stationary, and the process is dynamic.

Study of weld microstructure is essential for estimating the quality of the weld and the shape of heat input. Cormier et al. [4] presented results for microstructural behaviour of H13 steel produced via EB melting. They observed the presence of localised non-homogeneities along the boundary between the part's exterior contours and central squares. Blacha et al. [5] reported microstructural studies and mechanical characterization of EB welded joints of high strength alloys. They performed their study aiming to find correct parameters for producing good quality EB welds. For describing the geometry of weld cross-section,

1   DEPARTMENT OF MECHANICAL ENGINEERING, INDIAN INSTITUTE OF TECHNOLOGY KANPUR, KANPUR, 208016, UTTAR PRADESH, INDIA
2   MEMBRANE SCIENCE AND SEPARATION TECHNOLOGY DIVISION, CSIR-CENTRAL SALT AND MARINE CHEMICALS RESEARCH INSTITUTE, GB MARG, BHAVNAGAR, 364002, GUJARAT, INDIA

*   Corresponding author:arvindkr@iitk.ac.in
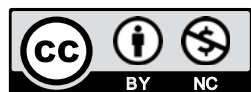
Yajun et al. [6] provided a novel concept of shape factors of the fusion-solidification zone. The weld fusion-solidification zone was divided into various shapes according to the obtained shape factors. Vishwakarma et al. [7] examined microstructures in FZ and HAZ of EB welded superalloy 718PLUS[TM]. The microstructural examination of the HAZ showed resolidified eutectic on the cracked and backfilled grain boundaries. Parthasarathy et al. [8] carried out the microstructural and mechanical characterization of the porous Ti6Al4V structures prepared using the EB melting process. The microstructure studies indicated complete melting of the powder material with no evidence of weak interlayer bonding. Chen et al. [9] conducted EB welding experiments on molybdenum and studied the weld microstructures, mechanical properties and defects of the joints. They concluded that average hardness of the weld was higher than that in the HAZ. They also observed that grains of HAZ and weld coarsened due to the high heat input of EB. Winczek [10] reported a full analysis of thermomechanical states during multipass weld surfacing by taking into account the relevant interactions between fields: temperature, phase transformation and stress. He concluded that the stress distributions are characterized by high values of tensile stresses in the weld and the HAZ, whereas in the base metal compressive stresses dominate and have a uniform linear distribution concerning the section height.

Some noticeable advances have been made in the existing concepts of solidification in recent years to describe nucleation, growth, and solute redistribution in HAZ and FZ, which helped in better description of weld properties. Significant advances have been made in the existing solidification theories in recent years to describe growth, nucleation, and solute redistribution in HAZ and FZ, which helped in better describing the weld properties. Ho [11] analytically investigated the effect of EB focusing characteristics on FZ. As a very significant work, their results revealed that a focused beam with small focal spot size and beam-convergence angle could induce a deep and narrow FZ. Zhuk et al. [12] investigated the effect of ingot heating conditions on the evolution of Ti-6Al-4V ingot macrostructure and surface quality during solidification which was subsequently processed by EB melting of via prototype production trials. They found that the preheating and post-heating helped to decrease the temperature gradient of welding heating and cooling cycles. It improved the uniformity of the temperature distribution in EB welding. Kim et al. [13,14] reported unusual microstructures during EB induced phase transition of aluminium trihydroxide. They observed that the pore's shape and crystals in the porous structure were decreased when the electron dose was increased. David and Vitek [15] provided a comprehensive review of the weld pool solidification behaviour in terms of solidification and microstructure. They correlated solidification parameters that control the weld pool solidification. Growth rate, temperature gradient and resultant interface undercooling were correlated with the weld microstructure. Nahmany et al. [16] studied the effect of heat input in the EB welding process and found that HAZ was very narrow. They found improved welding quality and weld morphology with beam oscillation. Yadav et al. [17] examined welded samples and revealed prominent grain growth in the HAZ and fine and equiaxed grains in the FZ.

EB welding is a very efficient and precise welding method used widely in industrial manufacturing. EB welding can be an effective method to process the Vacoflux-49 alloy. With the conventional welding processes, defects such as microcracking, caused by quenching of elements with different eutectic points, tend to occur in high precipitation-hardenable alloys. For counteracting cracking in these alloys the rapid temperature cycle is combined with high chill rates that are typical in EB welding., this also helps to reduce shrinkage. The lack of literature on EB processing of Vacoflux-49 alloy motivated us to study EB processing for this alloy. Chen et al. [18] successfully welded Ti-43Al-9V-0.3Y (at%) and Ti-6Al-4V (at%) alloys by EB to investigate the microstructure evolution of the joints. The results showed that the casting structure is formed during the solidification process of the weld, which inevitably causes component segregation in some parts of the joint.

Vacoflux-49 (Fe-49% Co-49% V-2%) is an essential member of the Fe-Co alloy family and is a semi-hard magnetic material. Sourmail [19] found that with the addition of vanadium to Fe-Co system, it is possible to import sufficient ductility for cold-rolling and hence to develop applications as laminated products. Fe-Co-V is known for excellent magnetic properties at elevated temperature and has low coercivity, high permeability, high tensile strength, high Curie temperature, high magnetization and low core loss. Having excellent mechanical properties along with high-temperature stability of magnetic properties, these alloys are particularly irreplaceable for making torque sensors, force sensors, sonar transducers and the active parts of the rotor of synchronous hysteresis motors [20].

In this work, experimental studies of EB spot melting and continuous welding of Vacoflux-49 are performed to understand the shape, size and microstructure of different zones formed. The experimental studies on melting have been carried out with under-focussed, focussed, and over-focussed beam and the resulting melt pool characteristics have been delineated. For focussed beam, the solidified melt pool in terms of shape, size and microstructures of different zones are examined. Subsequently, EB continuous welding is performed to join two plates of Vacoflux-49 as butt-joint, and the weld characteristics are investigated.

2. Experimental procedure and material

Spot melting and continuous welding experiments with Vacoflux-49 (Fe-49% Co-49% V-2%) material were performed using an EB welding machine, MEDARD 43 (make: Bodycote Techmata, France). The experiments were performed by employing a vacuum level of 10^{-8} mbar for the gun and 10^{-6} mbar for the chamber. The equipment has a viewing lens and a camera to ascertain the beam position for checking the

path before processing, and to monitor the beam if necessary. The specification of the machine is given in Table 1. Vacoflux-49 is a soft magnetic material with high Curie temperature, high saturation magnetization and low coercivity. It was invented by White and Wahl [21]. Due to its excellent magnetic properties, it is used in torque, sonar and gyroscopic sensors and many more high-temperature applications. Energy Dispersive X-Ray Spectrometry (EDS) analysis of as-received Vacoflux-49 has been carried out to obtain its chemical composition (see Fig. 1 and Table 2). There was a small amount of carbon present in the as-received material. In the melting experiments, circular bar (50 mm diameter and 10 mm length) of Vacoflux-49 was used. The sample size in EB welding experiments was 25 mm × 15 mm × 2.5 mm. The spot melting and welding experiments were performed using the parameters listed in Table 3 and Table 4, respectively.

TABLE 1

Specifications of electron beam welding equipment used for experimentation

Specification	Value
Beam current (I)	0-100 mA
High voltage (U)	0-60 kV
Focussing current (J)	0-4 A
Feed (F)	1000 mm s^{-1}
Chamber size	350 mm × 350 mm × 350 mm
Axes	3-axes (X, Y and C)
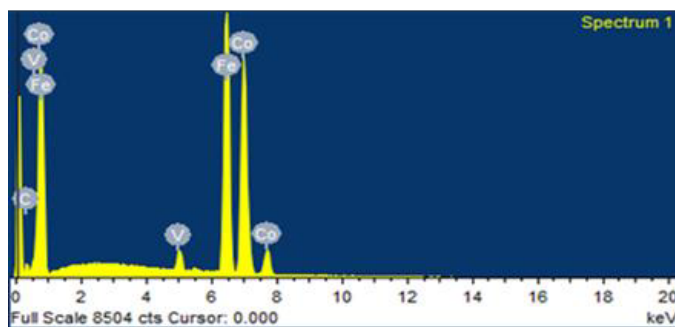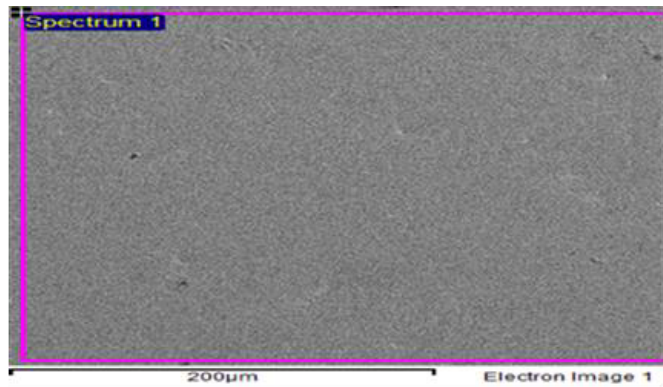
Fig. 1. EDS analysis of Vacoflux-49

Three sets of experiments were performed for each parameter under the same conditions to achieve the repeatability of results. After conducting melting and welding experiments on

TABLE 2

Chemical composition of Vacoflux-49 obtained by EDS analysis of as-received Vacoflux-49 from the supplier

Element	Weight %	Atomic %
Fe	48.32	47.65
Co	48.41	50.31
V	1.96	1.76
C	1.31	0.28
Total	100	100

TABLE 3

Parameters for electron beam melting experiments

Case	Beam voltage (kV)	Beam current (mA)	Beam power (W)	Duration of beam application (s)
Case I – under-focussed	55	25	1375	0.5
Case II – over-focussed	55	40	2200	0.8
Case III – focussed	55	30	1650	0.6

TABLE 4

Parameters for electron beam butt welding experiments

Case	Beam voltage (kV)	Beam current (mA)	Beam power (W)	Welding speed (mm s^{-1})
Case IV– butt welding	50	15	750	13.33

Vacoflux-49, standard polishing and etching techniques were used to reveal the HAZ, PMZ, FZ and meltpool geometry. Dino-Lite AM4111T digital USB microscope was used for analyzing the shape and size of the melted and re-solidified region. Optical electron microscope (OEM) (Brand – InTouchScope™Model number – JSM-6010LA) and scanning electron microscopy (SEM) (Brand – Carl Zeiss Model Number – EVO18 Special Edition) were used for microstructural analysis. The micrography was performed to reveal microstructure and shape of various features including grains, phases, embedded phases and embedded particle. Hardness test has been conducted on the EB melted sample using a universal hardness testing machine (Brand – Tinius-Olsen Ltd. Model number – FH-10)

3. Results and discussions

EB processing depends on various input parameters, such as voltage, beam current, focussing current, shooting distance, and takt time etc. Focus intensity is dependent on the shoot distance (firing distance, the distance between part and focussing coil), the focussing current, the accelerating voltage and the nature of the material. The size of the focus spot is determined

by the position of the EB focus point. High energy density lies in the spot, and the shape of the melt pool depends upon the position of the focus point. In the current study, the following cases have been considered:

Case I: Electron beam melting on Vacoflux-49 material with under-focussed beam.

Case II: Electron beam melting on Vacoflux-49 material with the over-focussed beam.

Case III: Electron beam melting onVacoflux-49 material with focussed beam.

Case IV: Electron beam butt welding of Vacoflux-49 material.

3.1. Shape and size of the solidified meltpool

3.1.1. Case I: Under-focused electron beam melting

If the EB is set to focus above the surface of the workpiece, then this is the case of the under-focussed beam. The macrostructure of the sample obtained with the help of Dino-Lite USB camera after melting and re-solidification with the under-focussed EB with parameters corresponding to data set #1 of Table 3 is shown in Figure 2. The shape of the re-solidified meltpool is hemispherical with depth 4.30 mm and width 11.88 mm. As can be seen, no evaporation zone is observed since the power is low and the beam is not focussed.
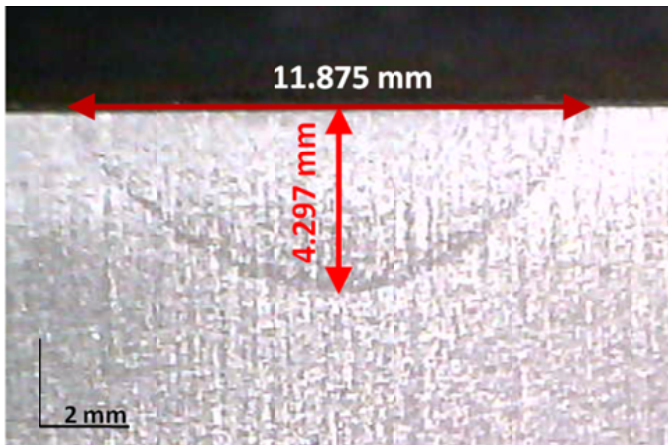
Fig. 2. Resolidified zone for case of under-focused beam melting experiment

3.1.2. Case II: Over-focused electron beam

If the EB is set to focus below the surface of the workpiece, then this is the case of the over-focussed beam. The macrostructure obtained after melting and re-solidification with an over-focussed beam of the sample with parameters corresponding to data set #2 of table 3 are shown in Figure 3. Similar to under-focussed EB, the shape of the re-solidified zone, is also hemispherical. However, its size (depth 3.75 mm and width 9.94 mm) is smaller than in Case I. No evaporation zone is observed as the power is low, and the beam is not focussed.
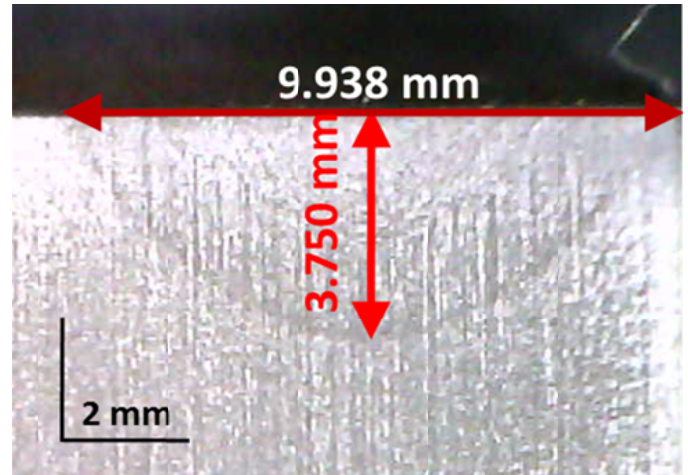
Fig. 3. Resolidified zone for case of over-focused beam melting experiment

3.1.3. Case III: Focused electron beam

If the EB is set to focus at the surface of the workpiece, then this is the case of the focussed beam. Focussed EB with parameters corresponding to data set #3 of table 3 was applied to the sample for 0.8 s. The macrostructure obtained with the help of Dino-Lite USB camera after melting and re-solidification is shown in Figure 4. As seen from Figure 4, at the point of the strike of EB metal gets evaporated, and the evaporated region is in the form of a cone. Chiumenti et al. [22] suggested that for the uniform beam, the evaporated material comes from a circle of radius $r_{ev} = 0.4r$, where r is the beam radius.

From the measured dimensions of the evaporated zone in this study, it was found that $r_{ev} = 0.63r$. Peripheral melted
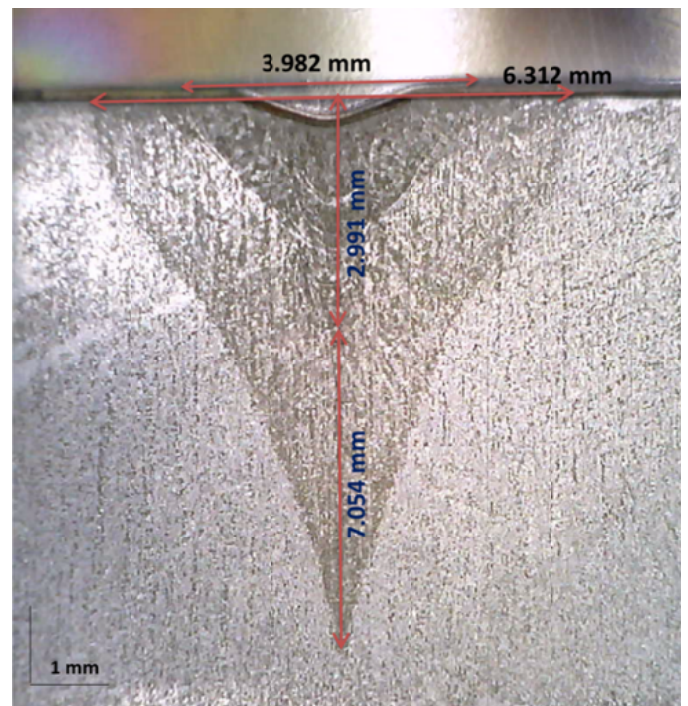

Fig. 4. Resolidified zone for case of focused beam melting experiment

material surrounding the evaporated cone creates the FZ on re-solidification. The portion surrounding the FZ is called partially melted zone (PMZ). The temperature of the PMZ is higher than the solidus temperature and below the liquidus temperature of the alloy. The shape of FZ and PMZ is like a choked funnel. This shape of FZ reflects actual 'nail-shaped' FZ typical for EB melting with high power [23, 24]. The size widths and depth of various zones are shown in Figure 4. Since more heat is added in the meltpool in the focussed beam case (Case III), the meltpool shape changes from hemispherical (Case I, II) to a deep funnel shape.

3.1.4. Case IV: Continuous butt welding

Depending on beam power, welding velocity, and focusing parameters the size and shape of FZ are essential factors determining the weld quality during EB welding. In the case of EB welding (Case IV), two plates of dimension 25 mm × 15 mm × 2.5 mm are butt welded with welding parameters as given in Table 4. It was blind welding, i.e., the partial thickness of the plate was welded. The shape of the weldment cross-section is shown in Figure 5a, which is very similar to the shape found in spot melting and re-solidification (Case III). Here also the shape is like a choked funnel. Figure 5b shows the top-view of the continuous EB butt welding. The dimension of the weldment cross-section is given in Figure 6. The width and the depth of the FZ were 0.91 mm and 0.75 mm, respectively.

(a)

(b)
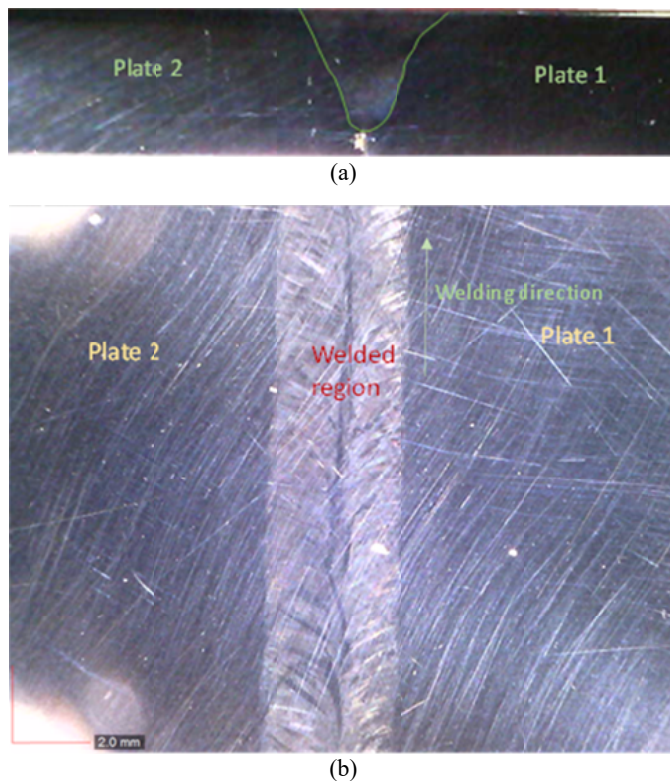
Fig. 5. Experimental image of continuous electron beam butt welding (a) cross-sectional view (b) top view
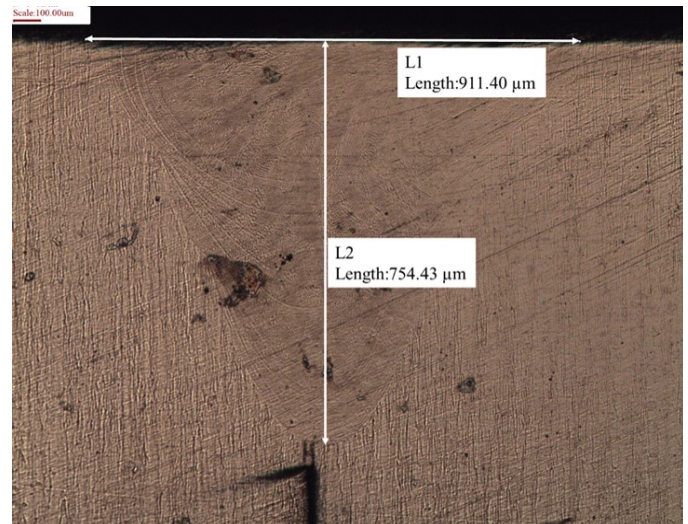
Fig. 6. Resolidified zone for case of continuous electron beam welding in cross-sectional view

3.2. Microstructure

3.2.1. Electron beam spot melting

For investigating the microstructural changes and the grains formed and their growth in FZ in electron beam melting, Case III (melting with focussed beam) is chosen. The top surface of the sample was first studied with the help of optical electron microscope. Figure 7 shows the microstructural image of FZ at the top surface. As seen in Figure 7, cellular columnar grains in spike pattern are formed radially which is caused due to microsegregation created between the cells [25] .
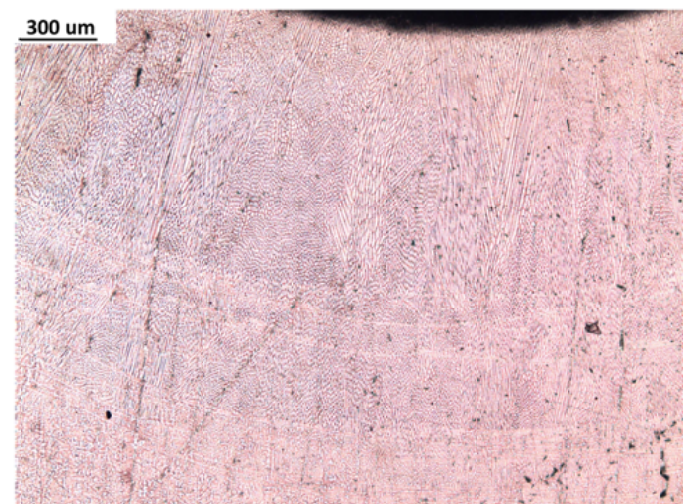
Fig. 7. Microstructural image of FZ at top surface for case of focused beam melting experiment

A schematic diagram of the cross-section of the sample used in Case III is shown in Figure 8a. Regions 1-4 in Figures 8b and 8c represent the locations of microstructural analysis. SEM image of FZ reveals a captivating wavy nature of FZ (see Fig. 9a-b).
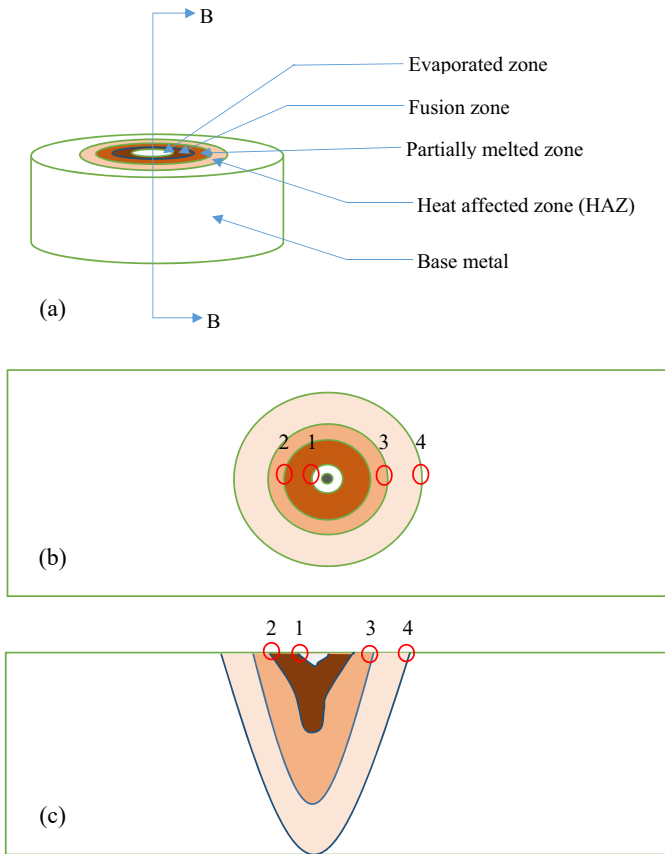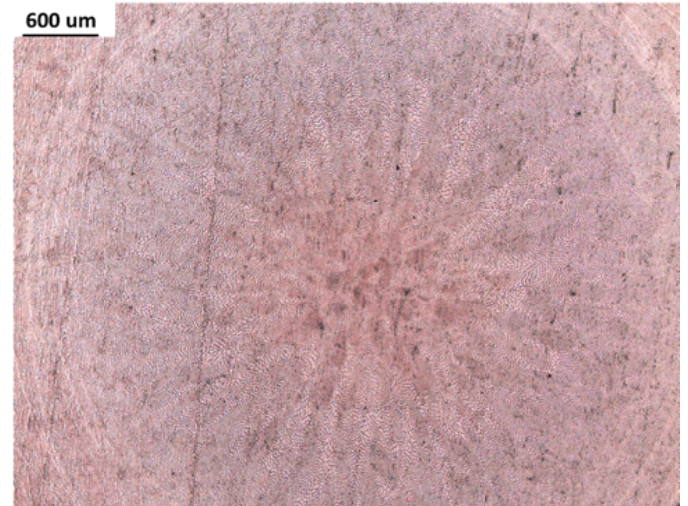
(a)

(b)

(c)

Fig. 8. Schematic diagram of the samples used in electron beam melting experiments (a) melted and re-solidified sample (b) top view (c) sectional view (B-B)
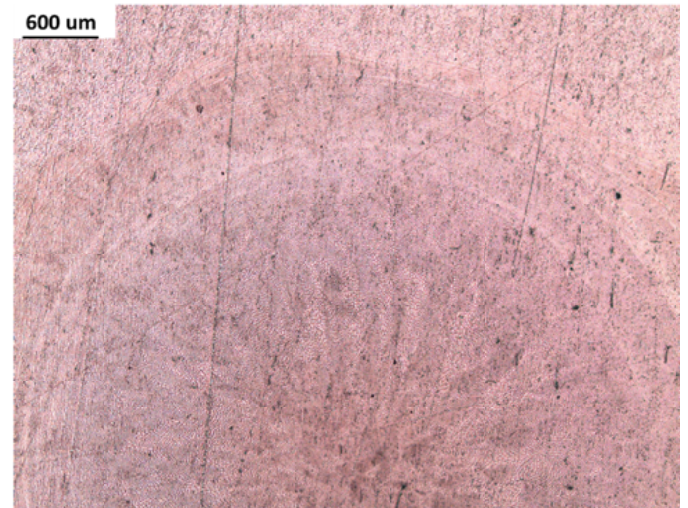

(a)

(b)

Fig. 9. (a) Wavy pattern grain growth at the centre of fusion zone in case of focused beam melting (b) Zoomed view of the solidification ring obtained in FZ

Crest and trough can be clearly observed in FZ. It can also be seen that at the crest the grains are coarse and large, while at the trough the grains are fine. This is because irradiation of electrons on the workpiece induces rapid heating with high-temperature gradients leading to shock waves at the top surface of the workpiece. Qin et al. [26] suggested that the presence of these shock waves causes thermal stress in FZ, which results in wavy nature of grain growth in FZ. Figure 9 shows the microstructure in region 1, as marked in Figures 8b and 8c. Fine grains at the centre and coarser grains near the base metal are observed. The grain type and the growth depend upon the solidification mode and the cooling rate, respectively. As the cooling rate is high at the centre, fine grains are found at the centre. In a similar way, the lower cooling rate towards the fusion front leads to coarser grain at those locations [27]. The relation between temperature gradient and growth rate at the centre line and the fusion line is given by [28].

$$(GR)_{CL} \ll (GR)_{FL} \qquad (1)$$

In Eq. 1, GR refers to the cooling rate, which dictates the arm spacing between the dendrite. In Eq. 1, the subscripts CL and FL refer to centre and fusion line, respectively. With an increase in the cooling rate, the dendrite arm spacing decreases. The cooling rate at the centre is higher than that at the fusion line. Hence, the arm spacing decreases from the fusion line to centre line.

Figure 10 shows a closer view of the solidification ring after removal of 0.1 mm material from the top surface. Electron beam is produced by heating a high melting point metal such as tungsten or tantalum-containing cathode. Electrons detach from cathode at high temperature and gather around it. Hence, the electric field is created to accelerate these electrons and direct them toward the workpiece. The anode is set to earth potential, and a negative voltage is applied to the cathode. Thus the flow of electrons is from cathode to anode in the form of ring shape towards the workpiece [27]. EB through the anode has sufficient velocity, but it lacks the required power density. Hence, to achieve the required high-density power, the beam is passed through an annular coil that produces a magnetic field which focuses the electrons. The penetration depth is highest for the case of the focused beam. Therefore, the solidification rings in the microstructure can be attributed to the ring-shaped flow of the electrons and hence energy, and are only present in the case of the focused beam.
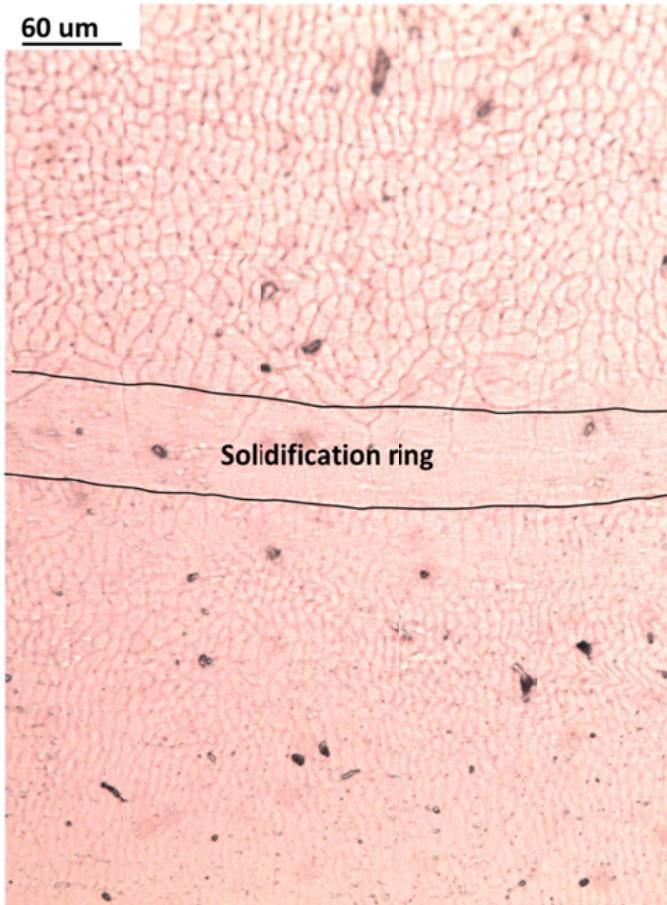
(a)

(b)

Fig. 13. (a) (a) Microstructural image at boundary of PMZ and FZ (b) Zoomed image at the boundary PMZ and FZ

(a)

(b)

(b)

Fig. 14. FE SEM image of (a) FZ (b) zoomed view of end part of FZ (c) zoomed image of Fig. 13a at the portion marked with the square box
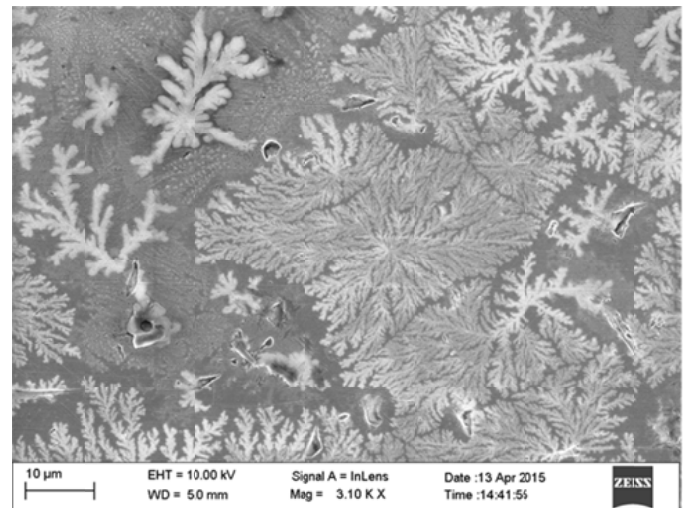
3.2.2. Electron beam welding

The grain growth in continuous welding is very similar to that in spot melting. Solidification ring in continuous welding is in the shape of an arc which started from the fusion front and diminished towards the centre line, as shown in Figure 15a. Fusion front is formed with overlapping of circular arcs made due to the movement of EB. The grains in the FZ are typically mix of planar, cellular, columnar dendritic and equiaxed dendritic [28]. Figure 15b shows mixed grain growth, which is a cellular type (fine and long). The grain structure is very similar to the focused spot melting case. The only difference is that in the case of continuous welding grains at the centre are long cellular as

shown in Figure 15b, while in case of spot melting the grains are fine cellular. FE-SEM image at the centre line shows the long cellular grain along the centre line and finer grain near to centre line. FE-SEM image of grain growth along the centre line is displayed in Figure 16, which shows long cellular grain along the centre line and finer grain near to centre line.
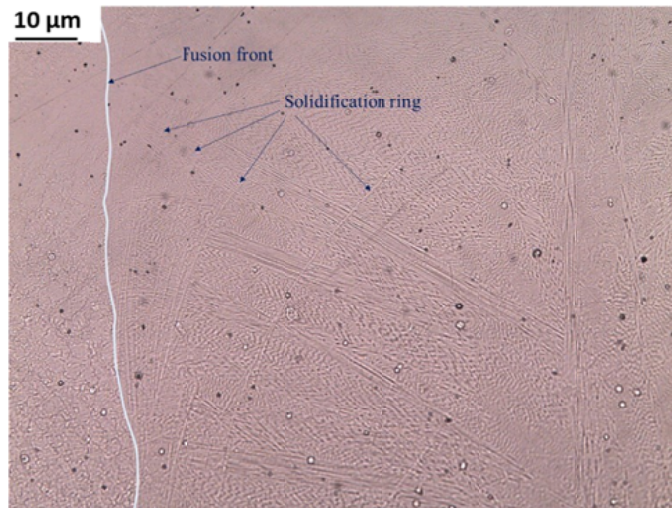
(a)
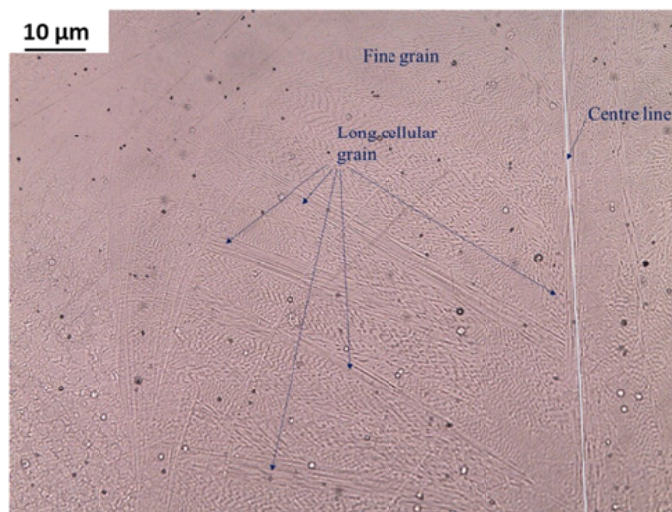
(b)

Fig. 15. (a) Fusion front and solidification ring in continuous electron beam butt welding (top view) (b) Grain growth in FZ
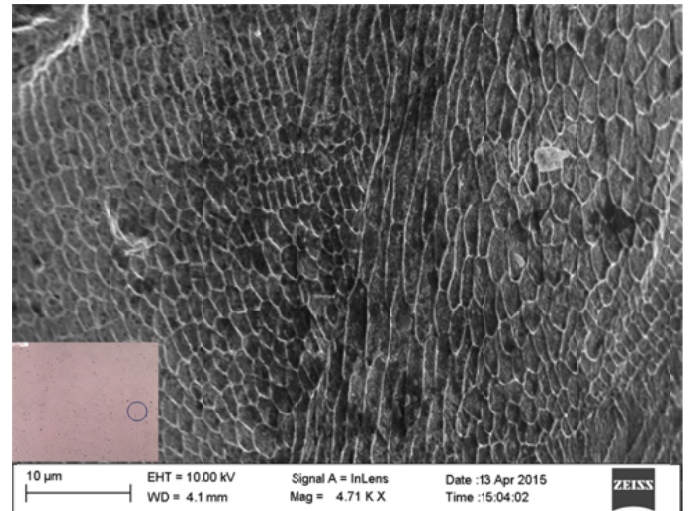

Fig. 16. FE-SEM image of grain growth along centre line in continuous electron beam welding

2. The grains in the fusion zone are typically mix of planar, cellular (fine and long), columnar dendritic and equiaxed dendritic. Spikes of long cellular grains are observed which started from fusion front and diminished at the center line. In general, finer grains at the centre and coarser grain near to base metal are observed.

3. Solidification rings in the microstructure of the fusion zone in the case of focused beam melting were observed, which can be attributed to the ring-shaped flow of the electrons.

4. The fusion zone grain structures appear wavy in nature.

5. The end portion of the choked funnel-shaped fusion zone shows dendritic structure.

6. The shape of weldment in the case of continuous welding is similar to spot melting case and appears like a choked funnel.

7. The grain growth in continuous welding is very similar to that in spot melting. The main difference is that the grain structure at centre line in the case of spot melting is fine and equiaxed while in the case of continuous welding, it is long cellular parallel to the welding direction. The solidification ring in continuous welding is in the shape of an arc which started from the fusion front and diminished towards the centre line.

4. Conclusions

Electron beam spot melting and welding experiments were carried out on sensors relevant Vacoflux-49 material, and shape, size, and microstructural feature of different zones formed were investigated. The following conclusions were drawn:

1. Electron beam spot melted region constitutes of four different regions, namely evaporated zone, fusion zone, partially melted zone and heat affected zone. The shapes of evaporated zone, fusion zone, partially melted zone and heat affected zone were elliptical, like a choked funnel, conical and conical, respectively.

REFERENCES

[1] D.H. Schultz, Electron beam welding, 1993 Abington publishing.

[2] R. Nakkalil, N.L. Richards, M.C. Chaturvedi, Acta Metall. Mater. **41**, 3381-3392 (1993).

[3] P. Petrov, C. Georgiev, G. Petrov, Vacuum **51**, 339-343 (1998).

[4] D. Cormier, O. Harrysson, H. West, Rapid Prototyp. J. **10**, 35-41 (2004).

[5] S. Błacha, M.S. Węglowski, S. Dymek, M. Kopyściański Arch. Metall. Mater. **62**, 627-634 (2017).

1156

[6] W. Yajun, F. Pengfei, G. Yongjun, L. Zhijun, W. Yintao, Chinese J. Aeronaut. **26**, 217-223 (2013).

[7] K.R. Vishwakarma, N.L. Richards, M.C. Chaturvedi, Mater. Sci. Eng. A **480**, 517-28 (2008).

[8] J. Parthasarathy, B. Starly, S. Raman, A. Christensen, J. Mech. Behav. Biomed. Mater. **3**, 249-59 (2010).

[9] G. Chen, J. Liu, X. Zhang, J. Feng, Vacuum **154**, 1-5 (2018).

[10] J. Winczek, Arch. Metall. Mater. **63**, 1615-1628 (2018).

[11] C.Y. Ho, J Mater. Process. Technol. **167**, 265-72 (2005).

[12] H.V. Zhuk, P.A. Kobryn, S.L. Semiatin, J. Mater. Process. Technol. **190**, 387-92 (2007).

[13] Y.M. Kim, S. Lee, Y.S. Kim, S.H. Oh, Y.J. Kim, J.Y. Lee, Scr. Mater. **59**, 1022-1025 (2008).

[14] Y.M. Kim, Y.S. Kim, S. Lee, Y.J. Kim, J.Y. Lee, Scr. Mater. **61**, 572-575 (2009).

[15] S.A. David, J.M. Vitek, Int. Mater. Rev. **34**, 213-45 (2014).

[16] M. Nahmany, I. Rosenthal, I. Benishti, N. Frage, A. Stern, Addit. Manuf. **8**, 63-70 (2015).

[17] A. Yadav, A. Ghosh, A. Kumar, J. Mater. Process. Technol. **248**, 262-274 (2017).

[18] G. Chen, G. Zhang, Q. Yin, B. Zhang, J. Feng, Mater. **233**, 336-339 (2018).

[19] T. Sourmail, Prog. Mater. Sci. **50**, 816-80 (2005).

[20] H. Mostaan, M. Shamanian, S.M. Monirvaghefi, P. Behjati, J.A. Szpunar, Vacuum **109**, 148-56 (2014).

[21] J.H. White, C.V. Wahl, Workable magnetic compositions containing principally iron and cobalt 1932.

[22] M. Chiumenti, M. Cervera, A. Salmi, C. Agelet, N. Dialami, K. Matsui, Comput. Methods. Appl. Mech. Eng. **199**, 2343-59 (2010).

[23] P. Lacki, K. Adamus, Comput. Struct. **89**, 977-85 (2011).

[24] P. Lacki, K. Adamus, K. Wojsyk, M. Zawadzki, Z. Nitkiewicz, Arch. Metall. Mater. **56**, 455-462 (2011).

[25] A. Hajitabar, H. N. Moosavy, Vacuum **150**, 196-202 (2018).

[26] Y. Qin, J. Zou, C. Dong, X. Wang, A. Wu, Y. Liu, H. Shengzhi, Q. Guan, Nucl. Instruments Methods Phys. Res. Sect. B Beam Interact. Mater. Atoms **225**, 544-54 (2004).

[27] A. Ghosh, A. Yadav, A. Kumar, J. Mater. Process. Technol. **239**, 52-65 (2017).

[28] S. Kou, Welding Metallurgy, 2nd Edition. 2003 John Wiley & Sons.